ADVANCED FUNCTIONAL MATERIALS
www.afm-journal.de

Materials Views
www.MaterialsViews.com

A Parallel Circuit Model for Multi-State Resistive-Switching Random Access Memory

*Albert B. K. Chen, Byung Joon Choi, Xiang Yang, and I.-Wei Chen**

Large, rapidly growing literature is available on bipolar resistive-switching random access memories (RRAM) made of myriad of simple and advanced materials. Many of them exhibit similar resistance switching behavior but, until now, no unifying model can allow quantification of their voltage and time responses. Using a simple parallel circuit model, these responses of a newly discovered RRAM made of a thin-film random material are successfully analyzed. The analysis clearly reveals a large population of intermediate states with remarkably similar switching characteristics. Such modeling framework based on simple circuit constructs also appears applicable to several RRAM made of other materials. This simple approach to analyze data write/rewrite and memory retention in RRAM may aid their further understanding and development.

1. Introduction

In the past decade, several new resistance-switching two-terminal devices have shown promise for future applications as resistive-switching random access memory (RRAM). Among them, non-phase-change RRAM is commonly found in oxide thin films, especially those of transition metal oxides including binary oxides (e.g., TiO_2,[1,2]NiO,[3] Al_2O_3,[4] ZrO,[5] SiO_2[6]), ternary oxides (e.g., $SrTiO_3$[7]) and quaternary oxides (e.g., (Pr,Ca)MnO_3[8]). Other materials such as amorphous-Si,[9] ionic conductors (e.g. Ag_2S)[10] as well as organic materials[11] were also reported to exhibit resistive switching behavior. Considerable progress in understanding these RRAMs has already been made. But there is still a need for a simple equivalent circuit model for quantifying their resistance (R)–voltage (V)–time (t) responses under fast as well as slow switching conditions. This model is developed here, in the hope that it will aid understanding of these devices and bring them closer to practical applications.

Our work focuses on a new family of nanoscale random materials for RRAM in which electron conduction is both size- and voltage- dependent. These properties were envisaged by Anderson since 1958,[12,13] but only recently were they realized in thin films made of atomic mixtures of insulating and conducting materials, wherein conduction is achieved over a short distance just enough to span the film thickness but not between different memory cells. RRAM of this construct has been demonstrated in widely disparate systems from single crystalline films ((Ca,Sr)(Zr,Ru)O_3, (Ca,La)(Zr,Ni)O_3, (La,Sr)(Al,Ru)O_3, and La(Al,Ni)O_3) made of random solid solutions of perovskite oxides to amorphous films of SiO_2 or Si_3N_4 with atomically dispersed Pt.[14,15] Within a window of composition and thickness, these structurally and chemically diverse films all exhibit the same type of I–V and R–V curves when the same electrodes are used [for example., Pt for the top electrode (TE) and $SrRuO_3$ (SRO) for the bottom electrode (BE)]. For amorphous films we also used Mo, which has a similar work function as SRO, as BE. Other than different BE resistance, R_{BE}, both devices behave similarly, so they will be used interchangeably in the following.) One such I–V curve and the corresponding R–V curve, taken from a 20 nm SiO_2:0.25Pt film, are shown in **Figure 1**a. It features counterclockwise hysteretic R–V switching, from a low-resistance-state (LRS, the "on"-state) to a high-resistance-state (HRS, the "off"-state). This occurs when the positive bias (applied to the TE relative to the BE) V_+ reaches a characteristic V_+* (called off-switching/transition). Conversely, the transition from the HRS to the LRS (called on-switching/transition) occurs when the negative bias V_- reaches a characteristic V_-* (see **Table 1** for a list of symbols). Note that V_+*>> V_-* for the first on-switching (1st V_-*) shown in Figure 1a; moreover, off-switching is sharp and abrupt occurring at a single V_+*, whereas on-switching is spread over several volts with several V_-* suggesting multiple transitions involving a multitude of intermediate-resistance-states (IRS). These IRS were also seen in other samples, one shown in Figure 1b, in which sweeps of different voltage amplitudes were used to better illustrate the mulple IRS. Note that each IRS apparently has its own V_+* that increases with the maximum V_- used (V_{max-}), however, the 1st V_-* seems to show no systematic trend and scatters around 1.2 V. Overall, the shape of the R–V curve in Figure 1a, including the existence of multiple resistance states, is not unlike the ones reported for many other bipolar RRAM. Therefore, we will use our random-material RRAM to develop a circuit model, which will explain (a) R–V curves for fast switching, (b) R–V–t curves for slow switching, and (c) nature and role of IRS in resistance switching.

One simplest circuit model for a two-point device is shown in Figure 1c), which views the resistive-switching film as n

Dr. A. B. K. Chen, Dr. B. J. Choi, X. Yang, Prof. I.-W. Chen
Department of Materials Science and Engineering
University of Pennsylvania
Philadelphia, PA 19104–6272, USA
E-mail: iweichen@seas.upenn.edu

DOI: 10.1002/adfm.201102208

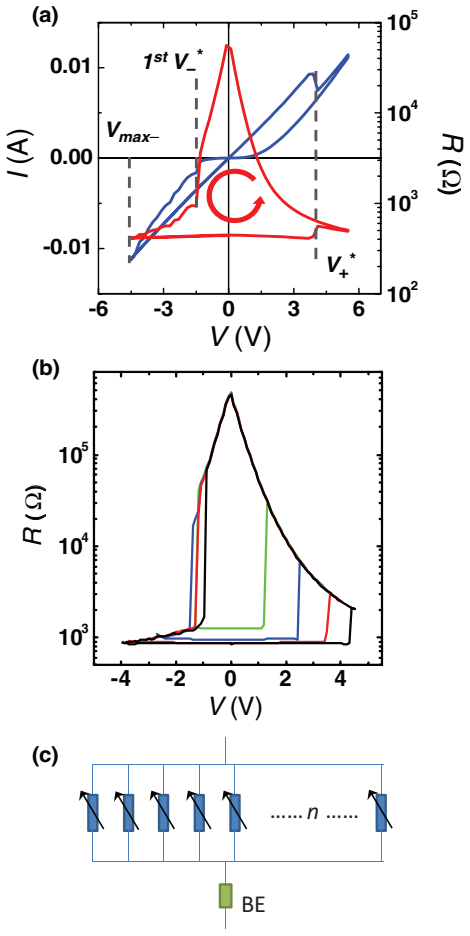

Figure 1. a) Current versus voltage (*I–V*, blue curve) and resistance versus voltage (*R–V*, red curve) of 25 nm SiO_2:0.25Pt RRAM device. Pt for top electrode (TE) and $SrRuO_3$ (SRO) for bottom electrode (BE). Ohmic for LRS, non-linear for HRS. The bottom electrode resistance (R_{BE}) of this cell is about 320 Ω. b) *R–V* curves with different sweep voltages V_{max-}. The magnitude of V_{max-} (4 V for black, 3.5 V for red, 2.5 V for blue and 1.3 V for green) determines the IRS, each of which has a well-defined Ohmic resistance (bottom of loop) and V_+* (right side of loop). Increase in V_{max-} decreases the Ohmic resistance and increases V_+*. Pt for top electrode and Mo for bottom electro. R_{BE} ~ 750 Ω. c) Schematic parallel circuit model, with *n* parallel, switchable elements in the film, in series with a constant resistance R_{BE} of bottom electrode.

parallel pathways, in series with an electrode resistance R_{BE}—in our device, the TE resistance is too small to be of concern. This model has one state variable *f*, the fraction of pathways that have a high resistance (each being R_H), the remaining ones have a low resistance (each being R_L). Reversible switching between R_H and R_L can occur on any pathway, which is assumed to be controlled by voltage. The total resistance made of R_{BE} and the (mixture) film resistance R_m (the second term in Equation 1)

$$R = R_{BE} + \frac{1}{f \cdot n/R_H + (1-f) \cdot n/R_L} \quad (1)$$

can thus vary between two limiting values, $R_{BE} + R_H/n$ and $R_{BE} + R_L/n$, which are assigned to the HRS ($f = 1$) and the LRS ($f = 0$), respectively. (Naturally, the IRS has an intermediate *f*.) It

Table 1. Symbols used for magnitude of voltage bias.

Symbols[a)]	Definition
V+	Positive bias on device
V–	Negative bias on device
V_{max-}	Maximum *V*– in sweep
V+*	*V*+ at off-switching
V–*	*V*– at on-switching
V_{m+}	Positive bias consumed in mixture film, at *V*+
V_{m-}	Negative bias consumed in mixture film, at *V*–
V_{m+}*	V_{m+} at off-switching

[a)]All are positive quantities representing magnitude only. Direction of bias is indicated by subscript: + (–) for positive (negative) bias of top electrode relative to bottom electrode.

turns out in our device $R_H >> nR_{BE} >> R_L$. Therefore, during on-switching from HRS to LRS nearly all the applied voltage (V_-) is consumed in the (mixture) film (V_{m-}) and not in the BE, i.e., $V_{m-} \approx V_-$, the latter equals V_-* upon switching. However, during off-switching from LRS to HRS the opposite holds, i.e., $V_{m+} << V_+$, the latter equals V_+* upon switching. This asymmetry provides a clue to why V_+*>> 1st V_-*. But to fully specify the circuit model, we also need the "true" switching threshold voltage V_{m-}* that triggers R_H-to-R_L on-switching in the film, and its counterpart V_{m+}* that triggers R_L-to-R_H off-switching. Since *f* is the only state variable, we expect $V_{+/-}$* as well as *R* and R_m to be functions of *f* only.

Our first goal is thus to determine these functions from experimental observations. In the following, we illustrate how this is achieved (Section 3) once a multitude of IRS is accessed (Section 2). We next present numerically computed *R–V* curves using these functions (Section 4). A further confirmation of our model in the *R–V–t* curves of time-dependent on-switching (Section 6) and off-switching (Section 5) leads to a retention-time prediction for the device. This is followed by a discussion (Section 7) of similar observations in other RRAM, before conclusions and a brief of the experimental methods.

2. Intermediate Resistance States

We previously demonstrated that the apparent resistance of the LRS can be progressively lowered by applying an increasingly larger negative bias, V_{max-}, which is the maximum negative voltage reached in the cycle.[15] In the current model, the term of LRS is designated to the $f = 0$ state, so we restate the above observation as follows: by increasing V_{max-}, an IRS of a smaller *f* can be obtained. (Physically, this is explained in our random material by charge detrapping driven by a negative bias that clears more pathways for electron conduction. However, the explanation is material dependent and is not essential for our phenomenological model.) As shown in Figure 1b, different IRS can be attained in the negative sweep using different V_{max-}, which then undergo off-switching at a sufficiently high V_+. Note that all these IRS have a voltage-independent resistance when the bias decreases, i.e., the IRS are all Ohmic. In this sense,

they can be regarded as "conducting states" since conductors such as metals typically have *V*-independent *R*. The resistance *R* shown as the horizontal section in Figure 1b) will thus be referred to as R_{cond}, which has a one-to-one correspondence to *f* in our model. Generally, increasing V_- can be used to switch one conducting state of a higher *f* (higher R_{cond}) to another conducting state of a lower *f* (lower R_{cond}), but lowering V_- will not cause any change in *f*. In contrast, the HRS in Figure 1b is obviously an "insulating state" in that its *R* is strongly *V*-dependent, like a typical insulator. Remarkably, regardless of R_{cond}, after off-transition there is only one *R*–*V* curve indicating a unique insulating state. This strongly suggests that the unique state is probably the $f = 1$ state, i.e., HRS. Lastly, since R_{cond} decreases with V_{max-}, reaching the true LRS ($f = 0$) apparently needs a very large, if not infinite, V_{max-}.

Experimentally, to gain access to different IRS, we can control either V_{max-} directly or through a current compliance. In the compliance control method, we first switch a device off to the insulating state under a V_+, then switch it on to a conducting state at a negative bias V_- under a current compliance. After that, V_- is reduced and the resistance read at ±0.2 V, at which the compliance is ineffective because the current is too small, thus not affecting *R*. The data of R_{cond} of the IRS attained at different compliance are shown in **Figure 2**a). These IRS are all non-volatile because $R = R_{cond}$ = constant at zero bias in Figure 1b.

To determine the V_+* for these R_{cond} states, we first remove the compliance and apply a *V*+. Switch-off occurs suddenly at a certain V_+* as shown in Figure 1b. These data are plotted in Figure 2b showing V_+* decreases with R_{cond}. We next subject the insulating state to an increasing V_- until its resistance drops (sometimes through several steps) to reach R_{cond}. This V_- is assigned as the V_-* for R_{cond}, which is plotted in Figure 2b. (To verify that V_+* is a function of R_{cond} (hence *f*) and independent of sweeping history, after reaching V_-*, we again reduce the bias and reverse it until off-switching occurs at V_+*. This value indeed coincides with the previously determined V_+*.) These experiments confirm that there are indeed many IRS, each with its own set of V_+^*, V_-* and R_{cond}. This is consistent with the idea of a single state variable *f*, which uniquely determines all the properties (V_+^*, V_-* and R_{cond}) of a given state. (Different *f* can be experimentally accessed by using different V_{max-} or $I_{compliance}$. Although neither experimental parameter is a state variable, under a fixed set of experimental condition it does have a one-to-one correspondence to *f*, hence to V_+^*, V_-* and R_{cond}.) It is remarkable that V_-* ~V_+* when they refer to the same *f*–R_{cond} state. This is unlike the strongly asymmetric relation noted in the Introduction. Therefore, the asymmetry in Figure 1a must have arisen because the *f*-state reached at V_-* is different from the *f*-state reached at the 1st V_+* during the voltage sweep of Figure 1a.

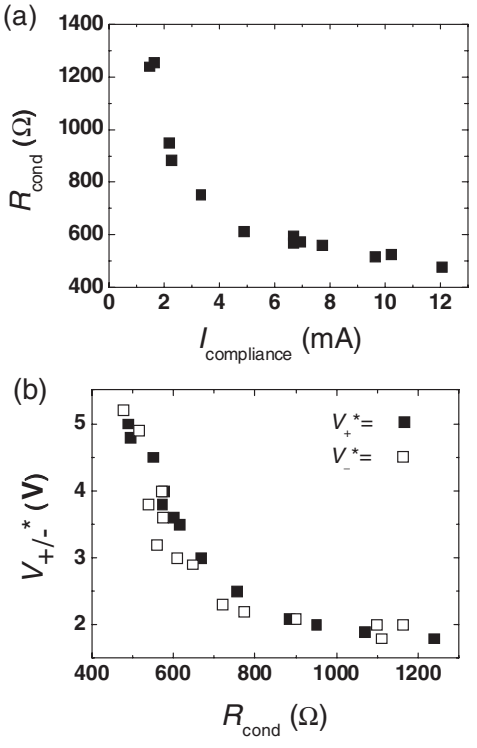

Figure 2. a) IRS resistance (R_{cond}) under different current compliance $I_{compliance}$ for negative voltage sweep to V_{max-} in Pt/SiO_2:0.25Pt/SRO device. R_{cond} read at 0.2 V. b) R_{cond} and its associated $V_{+/-}$* values. Pt for top electrode and SRO for bottom electrode. R_{BE} ~ 320 Ω.

The above results were obtained for SiO_2:Pt films with a Pt TE and a SRO BE. Essentially the same results were obtained if Mo BE is used, as shown in Figure S1 in Supporting Information, confirming again the existence of an IRS continuum. Other than these experiments, we further used an external load to "vary" the effective R_{BE}, and obtained the same results as above after factoring in the extra resistance. Because of voltage sharing, the *R*–*V* curve of the externally loaded device has a larger V_+* compared to an unloaded device.

3. Distribution of Switching Threshold Voltages

In Figure 2b, V_+* is as low as 1.5 V and as large as 5 V. Since a larger R_{cond} corresponds to a higher *f*, which in turn corresponds to a higher ratio of V_{m+}/V_+, the lowering of V_+* with R_{cond} does not necessarily imply a similar decrease in the actual threshold voltage, V_{m+}* required for switching the resistance element. To find the true switching threshold across the film, we need to assign the correct value to R_{BE}.

The circuit model and Equation 1) express the total resistance *R* in terms of R_{BE} and R_m. For conducting IRS, $R_{cond} = R_{BE+}R_m$ and is a function of V_-*. Expressing R_m as V_{m-}/I_-, where $-V_{m-}$ is the voltage in the film and $_I_-$ is the current at $_V_-$, we obtain

$$R_{cond} = R_{BE} + \frac{V_{m-}}{I_-} \quad (2)$$

This suggests that a plot of R_{cond} against $1/I-$ may reveal R_{BE}. This is because the plot yields a straight line if V_m- always reaches the same V_{m-}* each time when the transition (from a higher *f* to a lower *f*) occurs; i.e., if the switching threshold V_{m-}* is a constant. Even if V_{m-}* is not a constant, as long as it is a slow-varying function of *f*, we still expect a smooth R_{cond} vs. $1/I_-$ plot that can be extrapolated to $1/I_- = 0$ to determine the intercept, R_{BE}.

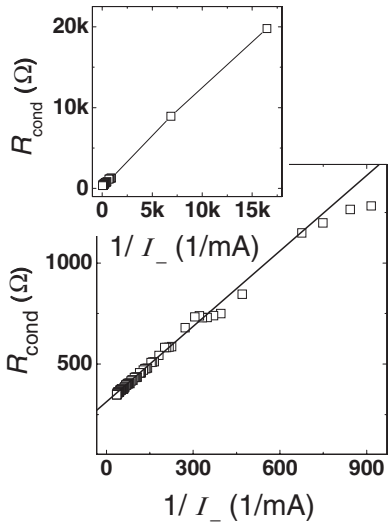

Figure 3. R_{cond} versus $1/I_-$ plot of a Pt/SiO_2:0.25Pt/SRO device, the extrapolated intercept gives R_{BE} about 320 Ω for SRO BE. Inset: more data over a larger $1/I_-$ range showing linearity.

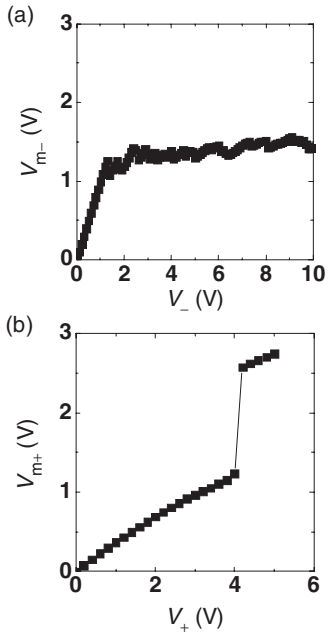

Figure 4. Voltages in SiO_2:0.25Pt film calculated using Equation 2. a) V_{m-} vs. V_- showing gradual up-ratcheting during on-transitions. b) V_{m+} vs. V_+ showing abrupt increase during off-transition. Pt for top electrode, SRO for bottom electrode. R_{BE} ~ 320 Ω.

To construct such R_{cond}–$1/I$ plot, we conducted tests up to a very high V_- and I_-. Measurements using a voltage ramp of up to ±20 V in the SRO BE films and up to ±10 V in the Mo BE films confirmed that R_{cond} is progressively lowered without affecting device's ability to switch: to the HRS under a V+. (A smaller voltage was used for Mo BE because Mo could oxidize under a large V_-.) The results plotted in **Figure 3** for SRO BE films nearly follow a straight line, with the slope steepening somewhat (indicating a larger V_{m-}*) at $1/I$–~0. The extrapolated intercept gives R_{BE} about 320 Ω for SRO BE (Figure 3). Similar data are shown in Figure S2 in Supporting Information for Mo BE.

Knowing R_{BE}, we can back-calculate V_{m-} from Equation 2 for each voltage sweep and reconstruct the true V_{m-} *vs.* V_- curve across the film, one of which shown in **Figure 4**a). Using the same R_{BE}, we can also compute V_m+ in the positive sweep and reconstruct the V_{m+} *vs.* V_+ plot, which is shown in Figure 4b. They have completely different shapes, which we explain below.

The V_{m-}-V_- plot has a saw-tooth, ratcheting top with many sharp peaks followed by steep drops, with the first drop occurring at V_- ~ 1 V which is the V_-* for the first resistance drop in Figure 1. Note that V_{m-}* ~ 1 V as well at this point. This is expected from Equation 1: the film is initially in the HRS, so the applied voltage is essentially all consumed in the film. However, after reaching the first V_{m-}*, V_{m-} suffers a sudden drop because R_m is now switched to a smaller value, hence the voltage sharing also drops to a lower value. It thus requires a higher V_- to return V_{m-} to the next V_{m-}* that triggers the next switching event. This process of "loading/unloading" repeats many times giving rise to the ratcheting shapes of the top, with each V_{m-} peak corresponding to a new V_{m-}*. Clearly, V_{m-}* is not a constant but a slow rising function of V_{max-}.

In contrast, the V_{m+}–V_+ plot follows a straight line until it suddenly rises at a V_+, i.e., V_+*. At this point, $V_{m+} = V_{m+}$* which is too ~1 V despite V_+* > 4 V. This is again expected from Equation 1: the conducting state has a R_m that is relatively small compared to R_{BE}, so the film only shares a small part of the applied voltage V_+. This plot also reveals the reason why off-switching is always abrupt and single-stepped: once V_{m+}* is reached, R_m increases rapidly so that V_{m+} also increases rapidly, which triggers further switching causing a further increase of R_m and V_{m+}. This self-reinforcing sequence sets up a chain reaction of successive switching, immediately bringing f to its upper limit of f = 1, i.e., the HRS. (The resistance of HRS rapidly decreases with voltage, as does V_{m+}/V_+, which is why the voltage in Figure 4b) only reaches 2.7 V, not 4 V, after the rise.)

In short, Figure 4a and b explain why the on-transition involves multiple steps and pauses at every IRS before proceeding to the next, but the off-transition is sharp and always reaches the same HRS in one step.

Although Figure 4a reveals many V_{m-}*, Figure 4b only reveals one V_{m+}*. However, if other sweeps with different V_{max-} are performed, then other V_{m+}* can also be collected, and such data can be plotted together against the compliance current or I_{max-}. This is shown in **Figure 5**a from which a distributed V_{m+}* emerges. Also, although Figure 4a already reveals a few V_{m-}*, more V_{m-}* can be found from other sweeps, and they can be pooled together to manifest the full distribution of V_{m-}* shown in Figure 5a) It is clear that V_{m+}* and V_{m-}* are of similar magnitude and generally increase with the compliance or I_{max-}, i.e., with decreasing f. Consistent with our expectation for distributed parameters, Figure 5a shows considerable scatter especially in V_{m-}*.

The above data are for cells with a SRO BE. Essentially the same trend is seen in the data for cells with a Mo BE (Figure 5b). Overall, it is clear that V_{m+}* and V_{m-}* are both distributed parameters, lying around 1 V.

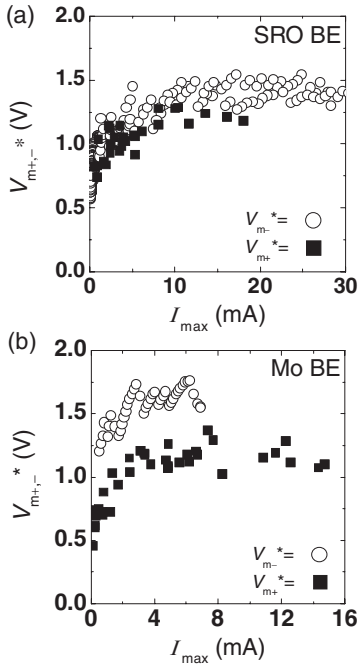

Figure 5. V_{m-}* and V_{m+}* values obtained for (a) Pt/SiO_2:0.25Pt/SRO and (b) Pt/SiO_2:0.3Pt/Mo device. V_{m-}* > V_{m+}*, both distributed around 1 V. Increasing I_{max-} corresponds to decreasing R_{cond} and f.

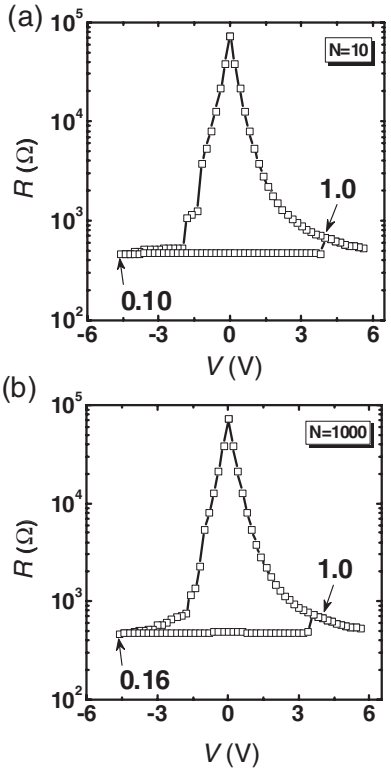

Figure 6. Computed *R–V* curves simulating Figure 1a (a SiO_2:Pt device) using parallel circuit model with $<V_{m+}*> = <V_{m-}*> = 1$ V, with a standard deviation of about 0.1 V. $R_{BE} = 320\ \Omega$, R_H/n given by Equation 3, $R_L/n = 140\ \Omega$, and $n = 10$ (a) and 1000 (b). The $V_{m+/-}$* for resistance elements are randomly generated following the same log normal distribution. As in Figure 1a, voltage sweeps in 0.2 V increment from 0 V to –4.6 V to 5.8 V to 0 V. Number indicates f on the curve at the arrowhead.

4. Computed *R–V* Hysteresis Curves

We are now in a position to compute the switching hysteresis curve using the circuit model with a realistic distribution of V_{m+}* and V_{m-}*. Because of the one-to-one correspondence between R_{cond} and f, it is possible to use the experimental data of Figure 5 to self-consistently derive the distribution as a function of f through a R_{cond}–f transformation using Equation 1. But this procedure is somewhat cumbersome and it is more convenient to simply assume a (log-normal) distribution with a mean value and a standard deviation, chosen in such a way as to fit the experimental *R–V* curve. In the following example, we treat n as a free parameter, and choose $<V_{m+}*> = <V_{m-}*> = 1$ V, with a standard deviation of 0.13. We also set $R_{BE} = 320\ \Omega$, and $R_L/n = 140\ \Omega$, to be consistent with the resistance of the LRS (~430 Ω, with $f \sim 0$) in Figure 1a. (At $f = 0$, $R = R_{BE} + R_L/n \leq 430\ \Omega$.) For R_H/n, we use the following form which numerically duplicates the *R*-– shape of the HRS.

$$\frac{R_H}{n} = R_0 \times \exp[-3.39883 \times |V| + 0.8022 \times |V|^2 - 0.05099 \times |V|^3 - 0.01004 \times |V|^4 + .00125 \times |V|^5] \quad (3)$$

Here, R_0 (72,550 Ω as in Figure 1a) is the resistance of HRS at 0 V. Two such calculated curves using $n = 10$ and $n = 1000$ are shown in **Figure 6**. The shapes of the calculated *R–V* curves are in obviously good agreement with the one in Figure 1, with the main effect of n being: the on-transition is more continuous for large n, and more discontinuous with multiple steps for small n. (Some discontinuities are caused by the finite voltage increment, 0.2 V, used in our simulation, as in our experiments.) It is also interesting to note the f value reached at the two ends of the voltage sweep: $f = 1$ at maximum V_+ and $f = 0.1$–0.16 at V_{max-}. This confirms our observation before: off-switching is always complete ending at the HRS which is unique, but on-switching is gradual and usually incomplete; becoming complete only at very large, if not infinite, V_{max-}. Further discussions of the best choice and physical meanings for n, R_H and R are material and device dependent and outside the scope of this work.

5. Time Dependent Switching of Multiple Resistance States: Off-Transition

We next consider constant-voltage stressing (CVS) tests which are often used to predict data retention.[16,17] In CVS, time-dependent switching is motivated by a sub-threshold voltage V_+ or V_- that is well below V_+* or V_-* used for fast write/erase of memory, and the data are recorded in the form of *R–t* plots as a function of sub-threshold voltage. Approximating $V_{m+/-}$* as a constant independent of f, we may interpret sub-threshold switching as a time-dependent change in f at a rate that is dependent on $V_{m+/-}$. This interpretation is taken below to analyze the CVS data.

For off-switching CVS, we first switch on a cell to a conducting IRS. For example, we choose a SRO BE cell with

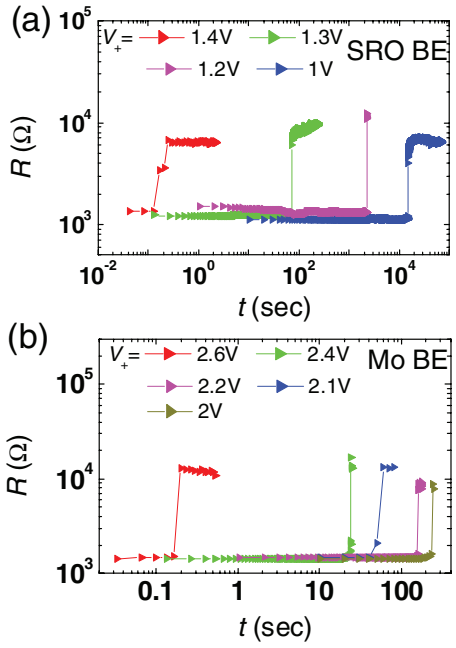

Figure 7. Resistance (R) versus time (t) under a constant voltage ($V+$) test (CVS test) of (a) Pt/SiO_2:0.25Pt/SRO, R_{BE} ~ 320 Ω and (b) Pt/SiO_2:0.25Pt/Mo device, R_{BE} ~ 750 Ω. All tests for the same IRS, with V_+* = 1.6 V in (a) and 3.5 V in (b); $V+$ for each curve specified in the upper margin.

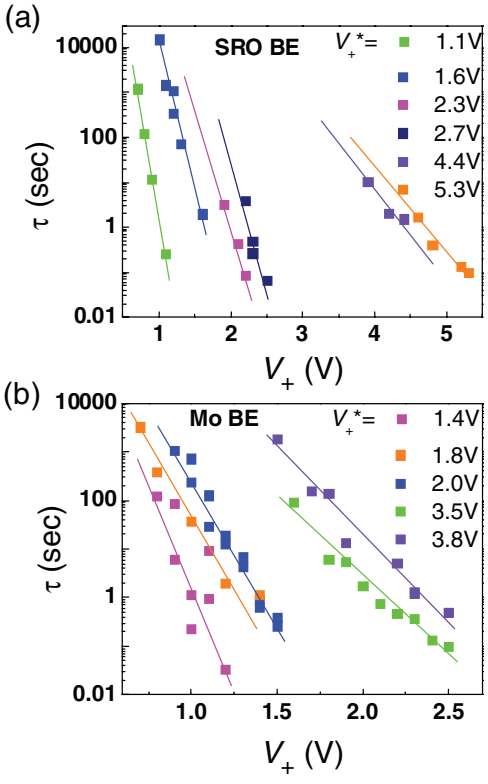

Figure 8. CVS switching time (τ) plotted against stressing voltage V_+ of (a) Pt/SiO_2:0.25Pt/SRO and (b) Pt/SiO_2:0.3Pt/Mo device. Each line corresponds to one IRS, labeled by its V_+* shown in the right margin.

a conducting IRS of R_{cond}~1 kΩ, which has a V_+* ~ 1.6 V according to Figure 2b). Next, a set of constant V_+ less than V_+* (e.g., 1 to 1.4 V) is applied. We then witness sub-threshold switching that manifests as a relatively sudden resistance rise over a relatively short duration around a switching time τ, as shown in **Figure 7**a. After repeating the test for other IRS of a different V_+*, we plot τ as a function of V_+ for each V_+*, which is shown in **Figure 8**a. Similar tests for a sample with a Mo BE show similar results, Figure 7b and Figure 8b.

As described in the previous sections, IRS differing in R_{cond} and R_m have rather different V_+* not because their V_{m+}* are very different but because their voltage sharing ratios, V_{m+}/V_+, are very different. This suggests that we should express the CVS results in terms of V_{m+}, instead of $V+$. Since the ratio V_{m+}/V_+, which equals R_m/R_{cond}, depends on R_m and R_{BE} only, and is the same for each IRS (i.e., V_+*) branch regardless of V_+ used, the re-plotting of the τ-log(V_+) data in terms of τ-log(V_{m+}) is equivalent to a (leftward) horizontal shift of the data along the log(V_+) axis by an amount of log(R_m/R_{cond}). Indeed, with such a shift we can bring the τ data of different IRS into overlap along a "master curve", shown in **Figure 9**a. Note that there is some scatter around the "master curve", which is expected since, after all, there is some distribution in V_{m+}*. (In this respect, we also note that there appears to be more scatter in the data with the highest V_+* in Figure 8. This is reasonable because the ratio V_{m+}/V_+ is the smallest in these least resistive films, which makes the V_{m+} in the constant-V_+ test most susceptible to noise.)

Data of CVS may be used to predict the reliability of a RRAM; the resistance value (memory) should remain stable over a time of the so-called retention time. In our random material RRAM, resistance switching is governed by charge trapping/de-trapping. With only a low, sub-threshold voltage available, we expect charge trapping/de-trapping will face a considerable barrier, and envisage Fowler-Nordheim tunneling (FNT) for moving electrons in and out of the trap through the barrier. The standard equation for FNT is

$$\frac{I}{V} = AV\exp(-\beta/V) \tag{4}$$

Here I is the current, A is a pre-exponential coefficient and β is a constant of the dimension of voltage. This equation may be rewritten as

$$\ln(\tau V^2) = \ln\frac{Q}{A} + \frac{\beta}{V} \tag{5}$$

after expressing I as Q/τ, with Q being a constant of the dimension of charge. The second form of the FNT equation suggests a linear plot in $\ln(\tau V^2)$ vs $1/V$. Replotting the data in Figure 9a in this way into Figure 9b, we are able to fit the data to obtain β. According to the literature,[18,19]

$$\beta = \frac{4(2m_{ox})^{1/2}d}{3e\hbar}\phi^{3/2} \tag{6}$$

Here, m_{ox} is the effective mass of electrons in SiO_2,[20] e is the elementary charge of an electron, $\hbar$ is reduced Planck's constant, ϕ is the effective barrier height, and d is the effective barrier thickness, which is unknown. If we use ϕ of 1 to 1.5 eV,

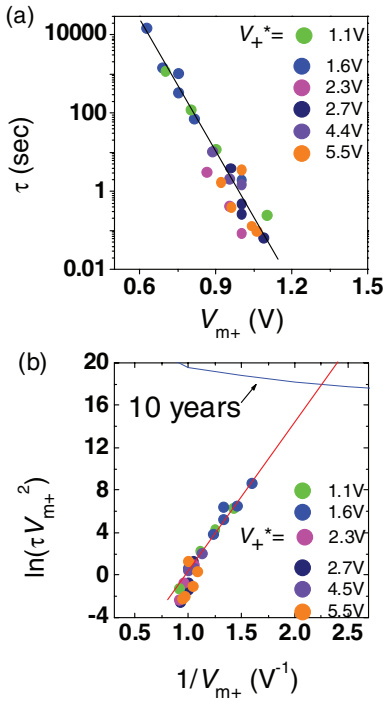

Figure 9. a) CVS switching time (τ) from Figure 8a plotted against actual stressing voltage on the film V_{m+} of a Pt/SiO_2:0.25Pt/SRO device. b) Same data in FNT plot motivated by Equation 5. Extrapolated intercept with the 10-year retention criterion indicates the maximum voltage V_{m+} allowed for reading is 0.43 V.

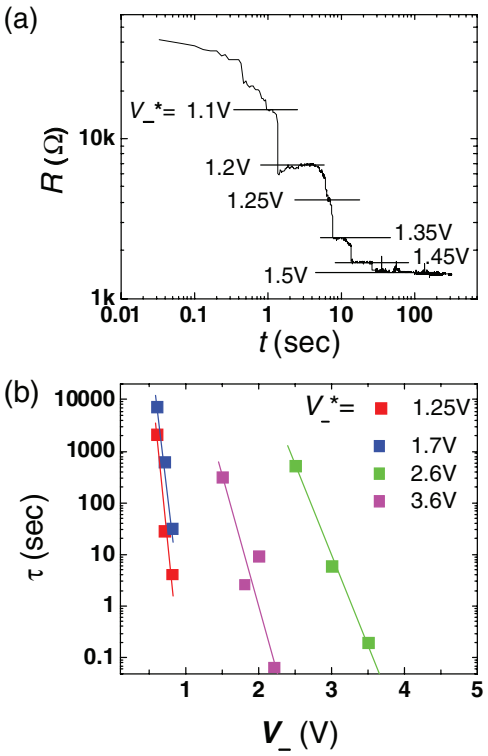

Figure 10. a) Resistance (R) vs. time (t) under a constant voltage (V_- = 0.8V) test of Pt/SiO_2:0.25Pt/SRO device. R_{BE}~ 320. Horizontal marker lines indicate the IRS with the corresponding V_-* specified next to lines. b) CVS switching time (τ) from (a) and other similar tests plotted against stressing voltage V_-. Each line corresponds to one IRS, labeled by its V_-* shown in the right margin.

which comes from V_m*, we find d to be 1.5 to 2.6 nm, which fits into our picture of nanometallicity.[14]

In Figure 9b, there is a gradual downward bend of the data toward the lowest $(V_{m+})^{-1}$, suggesting a rapid plunge of τ as the threshold voltage V_{m+}* is approached. This corresponds to fast switching; according to our study,[14,15] the V_+* hence V_{m+}* is independent of sweeping rate (as well as temperature), which is consistent with the notion of threshold voltage (it is not a memristor[1]). The existence of a threshold voltage implies another mechanism than FNT is operating at such large voltage. In our random material, we suggested the negative-U mechanism, which allows barrier distortion by way of localized atomic relaxation,[15] may operate at the threshold voltage.

During normal operation, a RRAM device is read by a small voltage. Common designs demand the device to sustain reading for 10 years without switching. This requirement is plotted in Figure 9b as a curve. Since the data line intersects with the curve at V_{m+} = 0.43 V, our standard read voltage of V_+ = 0.1 to 0.2 V will not cause any retention problem (note that $V_+ > V_{m+}$).

The above results are for SRO BE samples, but the same results are found in the Mo BE sample, as shown in Figure S3 in the Supporting Information.

6. Time Dependent Switching of Multiple Resistance States: On-Transition

To study on-switching CVS, the cell is first switched off to the HRS. Next, a negative bias V_- is applied to motivate resistance decrease over time. **Figure 10**a shows a test under −0.8 V, in which the resistance decreases in multiple steps, each rapid decrease followed by an incubation time before the next sudden decrease is triggered. We can identify these relatively constant resistance regions with the IRS, and read their characteristic V_-* from Figure 2b, some of which written next to the steps in Figure 10a. With this information, the data in Figure 10a can now be re-interpreted as (a) CVS of the HRS switching to the first IRS, i.e., the one that has the lowest V_-* and the highest R_m, and (b) successive CVS (at the same V_- = −0.8 V) of various IRS, switching to the next IRS, which has a higher V_-* and a lower R_m. Note that in (b), we should use the incubation time as τ. The test shown in Figure 10a can be repeated using other V_- (0.5 to −1 V). In addition, once a higher-V_-* step is reached, V_- can be reset to a higher value, and the CVS test continues. The data of different tests are next collated by grouping the τ-V_- data according to the V_-*, and the data for each V_-* are plotted in Figure 10b just like Figure 8 before. Again, these data are next replotted by considering V_{m-}/V_-, and the horizontally shifted data shown in the τ-log(V_-) plot in **Figure 11**a are further analyzed using the FNT plot in Figure 11b). Remarkably, the FNT plots of Figure 11b and Figure 9b are very similar (as are Figure 11a and Figure 9a). This suggests very similar barrier parameters in the FNT picture, which is not surprising in view of the similarity of V_{m+}* and V_{m-}*. Figure 11b also predicts a

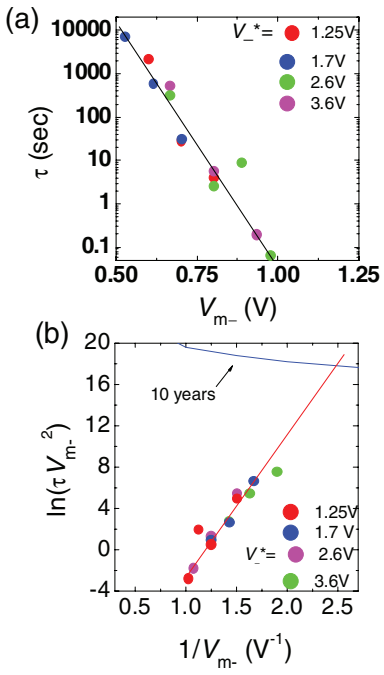

Figure 11. a) CVS switching time (τ) from Figure 10b plotted against actual stressing voltage on the film V_{m-} of a Pt/SiO_2:0.25Pt/SRO device. b) Same data in FNT plot motivated by Equation 5. Extrapolated intercept with the 10-year retention criterion indicates the maximum voltage (V_{m-}) allowed for reading is 0.4 V.

10 year retention if reading involves a $V_{m-} < 0.4$ V (note that $V_{m-} < V_-$, the actual read voltage).

The above results are for SRO BE samples, but the same results are found in the Mo BE sample, as shown in Figure S4 in the Supporting Information.

7. Discussion

We have used a parallel circuit model to analyze our SiO_2:Pt RRAM. Despite the simplicity of the idea, much insight has been extracted to the *I–V*, *R–V* and *R–V–t* behavior. Since other nanometallicity-based RRAM reported by us all share similar switching behavior as the SiO_2:Pt device,[14,15] we believe this model applies to them as well. We also believe this model could be applicable to some other RRAM unrelated to our devices.[21–31] For example, as illustrated in Figure S5, the *R–V* curve in a previous report[21] is very similar to the one shown in Figure 1, also exhibiting multiple on-transitions and an abrupt off-transition at a highly asymmetric, large voltage. (A similar observation on the same RRAM is reported,[22] although it used a configuration that caused a reversal of the voltage bias.) This suggests that the resistance transitions in the film material (amorphous InGaZnO) in this RRAM may also proceed along many parallel paths, even though the physical mechanism of resistance switching in this transparent thin-film-transistor material must be entirely different. An *R–V* curve very similar to that of Figure 6b, corresponding to the case of a very large n with a smooth on-transition and an abrupt off-transition at a highly asymmetric, large voltage was also seen in the RRAM made of another material (Cr-doped $SrTiO_3$) with trap-controlled space–charge-limited-conduction.[23]

Our model above is rested on the assumptions of (a) parallel conductor/resistor paths and (b) $nR_{BE} >> R_L$. But the analytical framework we provided is general and may be applied to other cases. For example, if (b) is not obeyed but the parallel circuit model still holds, then pronounced asymmetry and abrupt off-transition should be replaced by relatively symmetric on- and off-transitions that both have multiple steps; these transitions become more continuous (smoother) when n increases. We have seen such behavior in our work when R_{BE} is greatly reduced. (Indeed, this is the preferred situation to resolve multiple IRS.) In the literature, *R–V* curves of this kind have also been reported for several RRAM that have relatively high low resistance values, such as those with Schottky barrier-like interface (Nb-doped $SrTiO_3$),[24,25] or interface oxidation ((Pr,Ca)MnO_{3-x}).[8,26,27] If (a) does not hold but the film may still be regarded as n resistors in series, then it can be shown that R_{BE} is unimportant and the *R–V* curve always has multiple off-transitions (unless $n = 1$), but an abrupt on-transition at a highly asymmetric, large voltage, as seen in several RRAM (Cu/SiO_2, doped $SrZrO_3$, TiO_2, Ag/GeSe) that appear to follow the so-called filamentary mechanism.[28–31]

Although our model is based on voltage control, it turns out that the above discussion concerning the types of *R–V* behavior is still correct if the resistance transition in the same equivalent circuit condifuration is controlled by a threshold current or power. Therefore, the framework of equivalent circuit we proposed is quite general and robust, independent of the detailed, microscopic physical mechanisms. Analysis based on it may thus be used to provide essential insight, guiding further studies of the material physics of the device.

8. Conclusions

1) The resistance switching characteristics of nanometallicity-based RRAM have been successfully analyzed using a parallel circuit model taking into account the voltage-sharing effect of the bottom electrode.
2) The analysis reveals a rich population of intermediate states, corresponding to different fractions of the resistance elements that are either conductors or insulators. The threshold voltage for switching an individual element between the two states is about ±1 V.
3) Constant voltage stressing causes resistance changes occurring in multiple steps, interrupted by arrests at the intermediate states. Similar stressing kinetics holds for all the intermediate states due to the similar threshold voltage for switching individual resistant elements.
4) Constant voltage stressing tests confirm that the SiO_2:Pt RRAM can retain resistance memory for at least ten years. The slow memory lapse is consistent with a tunneling mechanism with a barrier thickness of approximately 2 nm.
5) As the modeling framework proposed here is seemingly applicable to several other RRAM reported in the literature, it may provide new analysis and understanding of their performance, thus aiding further development toward practical devices.

9. Experimental Section

Devices were grown on Si substrates covered with a thermally grown oxide. First, a bottom electrode (SRO by pulse laser deposition or Mo by DC sputtering) was deposited. Next, a SiO_2:Pt mixture film was deposited by radio frequency co-sputtering using targets of Pt and SiO_2. Finally, a Pt top electrode was deposited by sputtering through a shadow mask (typically 80 μm in diameter) on the mixture film. The composition of the SiO_2:Pt mixture films was measured by energy dispersive X-ray spectroscopy calibrated by Rutherford backscattering spectroscopy. All electrical measurements were conducted using a semiconductor parameter analyzer (SPA, Keithley 237). The sample was placed on a probe station and the voltage was applied to the Pt top electrode with the bottom electrode grounded. After fabrication, the device did not need a "forming process" to switch it to the low resistance state. During storage the devices were protected by a thin amorphous layer of Al_2O_3 coated by atomic layer deposition.

Supporting Information

Supporting Information is available from the Wiley Online Library or from the author.

Acknowledgements

This research was supported by the US National Science Foundation (Grant No. DMR-11-04530, primarily, and DMR-09-07523 and DMR-11-20901, in part.)

Received: September 16, 2011
Published online: December 7, 2011

[1] J. J. Yang, M. D. Pickett, X. Li, D. A. A. Ohlberg, D. R. Stewart, R. S. Williams, *Nat. Nanotechnol.* **2008**, *3*, 429.
[2] B. J. Choi, D. S. Jeong, S. K. Kim, S. Choi, J. H. Oh, C. Rohde, H. J. Kim, C. S. Hwang, K. Szot, R. Waser, B. Reichenberg, S. Tiedke, *J. Appl. Phys.* **2005**, *98*, 033715.
[3] C. B. Lee, B. S. Kang, M. J. Lee, S. E. Ahn, G. Stefanovich, W. X. Xianyu, K. H. Kim, J. H. Hur, H. X. Yin, Y. Park, I. K. Yoo, *Appl. Phys. Lett.* **2007**, *91*, 082104.
[4] S. Kim, Y.-K. Choi, *Appl. Phys. Lett.* **2008**, *92*, 223508.
[5] C.-Y. Lin, C.-Y. Wu, C.-Y. Wu, C.-C. Lin, T.-Y. Tseng, *Thin Solid Films*, **2007**, *516*, 444.
[6] C. Schindler, S. C. P. Thermadam, R. Waser, *IEEE Trans. Electron Devices* **2007**, *54*, 2762.
[7] K. Szot, W. Speier, G. Bihlmayer, R. Waser, *Nat. Mater.* **2006**, *5*, 312.
[8] Y. Chen, W. Tian, H. Li, X. Wang, W. Zhu, *IEEE Electron Dev. Lett.* **2010**, *31*, 866.
[9] K.-H. Kim, S.-H. Jo, S. Gaba, W. Lu, *Appl. Phys. Lett.* **2010**, *96*, 053106.
[10] T. Hasegawa, T. Ohno, K. Terabe, T. Tsuruoka, T. Nakayama, J. K. Gimzewski, M. Aono, *Adv. Mater.* **2010**, *22*, 1831.
[11] L. D. Bozano, B. W. Kean, M. Beinhoff, K. R. Carter, P. M. Rice, J. C. Scott, *Adv. Funct. Mater.* **2005**, *15*, 1933.
[12] P.W. Anderson, *Phys. Rev.* **1958**, *109*, 1492.
[13] E. Abrahams, P. W. Anderson, D. C. Licciardello, T. V. Ramakrishnan, *Phys. Rev. Lett.* **1979**, *42*, 673.
[14] A. B. K. Chen, S. G. Kim, Y. Wang, W.-S. Tung, I.-W. Chen, *Nat. Nanotechnol.* **2011**, *6*, 237.
[15] B. J. Choi, A. B. K. Chen, X. Yang, I.-W. Chen, *Adv. Mater.* **2011**, *23*, 3847.
[16] Y. S. Chen, H. Y. Lee, P. S. Chen, P. Y. Gu, C. W. Chen, W. P. Lin, W. H. Liu, Y. Y. Hsu, S. S. Sheu, P. C. Chiang, W. S. Chen, F. T. Chen, C. H. Lien, M. J. Tsai, *IEDM* **2009**.
[17] Z. Wei, T. Takagi, H. Ohta, Kouichi Ono, *Appl. Phys. Lett.* **2009**, *94*, 013507.
[18] J.W. Gadzuk, E. W. Plummer, *Rev. Mod. Phys.* **1973**, *45*, 487.
[19] J. M. Beebe, B. S. Kim, J. W. Gadzuk, C. D. Frisbie, J. G. Kushmerick, *Phys. Rev. Lett.* **2006**, *97*, 026801.
[20] E. H. Snow, *Solid State Commun.* **1967**, *5*, 813.
[21] M.-C. Chen, T.-C. Chang, S.-Y. Huang, S.-C. Chen, C.-W. Hu, C.-T. Tsai, S. M. Sze, *Electrochem. Solid-State Lett.* **2010**, *13*, H191.
[22] M.-C. Chen, T.-C. Chang, C.-T. Tsai, S.-Y. Huang, S.-C. Chen, C.-W. Hu, S. M. Sze, M.-J. Tsai, *Appl. Phys. Lett.* **2010**, *96*, 262110.
[23] B. T. Phan, C. Jung, T. Choi, J. Lee, *J. Kor. Phys. Soc.* **2007**, *51*, 664.
[24] H. Sim, H. Choi, D. Lee, M. Chang, D. Choi, Y. Son, E.-H. Lee, W. Kim, Y. Park, I.-K. Yoo, H. Hwang, *IEDM Tech. Dig.* **2005**, 758.
[25] T. Fujii, M. Kawasaki, A. Sawa, H. Akoh, Y. Kawazoe, Y. Tokura, *Appl. Phys. Lett.* **2005**, *86*, 012107.
[26] M. Fujimoto, H. Koyama, Y. Nishi, T. Suzuki, *Appl. Phys. Lett.* **2007**, *91*, 223504.
[27] Z. W. Xing, J. Wu, A. Ignatiev, *Appl. Phys. Lett.* **2007**, *91*, 052106.
[28] C. Schindler, S. C. P. Thermadam, R. Waser, M. N. Kozicki, *IEEE Trans. Electron Devices* **2007**, *54*, 2762.
[29] C.-C. Lin, C.-C. Lin, D.-C. Tu, J.-S. Yu, C.-H. Lin, T.-Y. Tseng, *Jpn. J. Appl. Phys.* **2007**, *46*, 2153.
[30] M. H. Lee, K. M. Kim, G. H. Kim, J. Y. Seok, S. J. Song, J. H. Yoon, C. S. Hwang, *Appl. Phys. Lett.* **2010**, *96*, 152909.
[31] S. Yu, J. Liang, Y. Wu, H.-S. P. Wong, *Nanotechnology* **2010**, *21*, 465202.